Kinesin-2 Differentially Regulates the Anterograde Axonal Transports of Acetylcholinesterase and Choline Acetyltransferase in *Drosophila*

Rehan Baqri,[1]* Rakshita Charan,[1]* Kristina Schimmelpfeng,[2] Swati Chavan,[1] Krishanu Ray[1]

[1] Tata Institute of Fundamental Research, Mumbai 400 005, India

[2] Center for Molecular Medicine, HHMI, UCSD, La Jolla, California 92093-0883

Received 14 June 2005; accepted 5 October 2005

ABSTRACT: **Choline acetyltransferase (ChAT) and acetylcholinesterase (AChE) are involved in acetylcholine synthesis and degradation at pre- and postsynaptic compartments, respectively. Here we show that their anterograde transport in *Drosophila* larval ganglion is microtubule-dependent and occurs in two different time profiles. AChE transport is constitutive while that of ChAT occurs in a brief pulse during third instar larva stage. Mutations in the kinesin-2 motor subunit *Klp64D* and separate siRNA-mediated knockouts of all the three kinesin-2 subunits disrupt the ChAT and AChE transports, and these antigens accumulate in discrete nonoverlapping punctae in neuronal cell bodies and axons. Quantification analysis further showed that mutations in *Klp64D* could independently affect the anterograde transport of AChE even before that of ChAT. Finally, ChAT and AChE were coimmunoprecipitated with the kinesin-2 subunits but not with each other. Altogether, these suggest that kinesin-2 independently transports AChE and ChAT within the same axon. It also implies that cargo availability could regulate the rate and frequency of transports by kinesin motors.** © 2006 Wiley Periodicals, Inc. J Neurobiol 66: 378–392, 2006

Keywords: **KLP64D; kinesin-2; axonal transport; acetylcholinesterase; choline-acetyltransferase; *Drosophila***

INTRODUCTION

Choline acetyltransferase (ChAT) and vesicular acetylcholine transporter (VAChT) are required for the synthesis and packaging of acetylcholine at the presynaptic compartment, and acetylcholinesterase (AChE), which is present at the postsynaptic membrane, hydrolyzes it (Parsons et al., 1993 for review). Genetic and pharmacological studies showed that block in ChAT, AChE, or VAChT activity by either mutations or antagonist treatments causes synaptic malfunctioning and paralysis in worms, insects, and humans (Engel et al., 1999; Kitamoto et al., 2000; Ohno et al., 2001; Suzuki et al., 2001). Experimental evidence also indicates that relative neuronal levels of these three enzymes are actively coregulated. For instance, the over-expression of AChE in mouse neurons elevates the levels of ChAT in these cells (Andres et al., 1997). The ChAT and VAChT gene-expressions are regulated by common upstream elements in *Drosophila* (Kitamoto et al., 1998) and in several other organisms (Berse and Blusztajn, 1995; Cervini et al., 1995; Oosawa et al., 1999).

Because all these enzymes are made at the neuronal cell body and localized at the synaptic terminals,

This article includes Supplementary Material available via the Internet at http://www.interscience.wiley.com/jpages/0022-3034/suppmat.

*These authors contributed equally to the manuscript.

Correspondence to: K. Ray (krishanu@tifr.res.in).

Contract grant sponsor: TIFR.

Contract grant sponsor: NIH; contract grant number: RO3 TWO5784 (K.R.).

Published online 11 January 2006 in Wiley InterScience (www.interscience.wiley.com).
DOI 10.1002/neu.20230

which in some cases could be several meters away, the anterograde axonal transport (AT) by microtubule-dependent motor proteins could play an important role in maintaining their proportional balance at the synapse. Independent studies have shown that AChE is transported bidirectionally while ChAT is mainly transported in the anterograde direction. The anterograde transport rate of AChE is nearly 10-fold faster than that of ChAT (Di Giamberardino and Couraud, 1978; Wooten and Cheng, 1980) and it requires microtubules (Kasa, 1968). However, the underlying mechanisms of their transports remain unknown.

Kinesin-2 is a member of the kinesin superfamily of microtubule-dependent motor proteins. It is a heterotrimeric complex of two motor subunits and a nonmotor accessory protein involved in anterograde intraflagellar transport (IFT), which maintains the cilia and flagella in several different cells (Sarpal et al., 2003; Rosenbaum and Whitman, 2002, for review). The motor subunits of kinesin-2 are also implicated in the AT in mouse and *Drosophila* (Yamazaki et al., 1995; Yang and Goldstein, 1998; Ray et al., 1999). The kinesin-like protein 64D (*Klp64D*) loci of *Drosophila* codes for a protein homologous to the kinesin-2 motor subunit KIF3A, and it expresses at a higher level in cholinergic neurons (Ray et al., 1999; Sarpal and Ray, 2002). Mutations in *Klp64D* cause selective accumulation of ChAT in axons (Ray et al., 1999) while KIF3A was shown to associate with small (≈50 nm) lipid-bound vesicles in sciatic nerve axons (Kondo et al., 1994). Although not quite explicitly demonstrated, this evidence indicates that kinesin-2 could be involved in anterograde AT of acetylcholine synthesis and recycling enzymes. Hence, this provided an opportunity to probe further the mechanisms of axonal transport of ChAT and AChE and to identify the role of kinesin-2 in these processes by using genetic analysis in *Drosophila*.

Here we present evidence to suggest that kinesin-2 subunits are involved in the AT of the acetylcholine synthesis and recycling enzymes in *Drosophila*. We have designed an assay to study the relative AT profiles of various presynaptic antigens in larval ventral ganglion and used it to analyze the roles of microtubule and kinesin-2 subunits in the anterograde transport of ChAT and AChE. Details of the experimental results and their implications are discussed below.

MATERIALS AND METHODS

Descriptions of all the fly stocks if otherwise not mentioned in this article are available in the fly-base (http://www.flybase.org), or in Lindsley and Zimm (1992). $Klp64D^{k1}$ and $Klp64D^{k5}$ are amorphic alleles of *Klp64D (*Ray et al., 1999). $Klp64D^{k1}$ contains a stop codon at the thirteenth amino acid position in the predicted ORF while $Klp64D^{k5}$ contains a missense mutation converting the 551 Glu to Lys. The UAS-KLP64D transgene contains the full length ORF as well as 435 base pairs upstream of the *Klp64D* gene. The transgene alone rescues the lethality of *Klp64D* alleles to a certain extent (Ray et al., 1999; S. Chavan and K. Ray, unpublished observation).

Immunostaining

Larvae were dissected in 4% formaldehyde in phosphate buffered saline (PBS; Sambrook et al., 1986) and fixed for 15–30 min in the same solution. Next, they were rinsed in PBS with 0.3% Triton X-100 (PTX) and incubated in primary antibody solution for 1 h, followed by washes in PTX with several changes, and further incubation in fluorescently conjugated secondary antibody solution in PTX for 1 h. Then the specimens were washed in PTX and mounted under a cover glass with a drop of Vectashield (Vector Labs Inc., USA). All images were collected using a Bio-Rad Radiance 2100 LSCM with identical laser power and detector settings and further processed using ImageJ (http://rsb.info.nih.gov/ij/) and Adobe PhotoShop. We used MAb4B1 at 1:1000 for ChAT (Takagawa and Salvatera, 1996), rabbit anti-Ace at 1:1000 for AChE (Incardona and Rosenberry, 1996), purified rabbit anti-VAChT (Kitamoto et al., 2000) at 1:200, both the mouse MAbs for anti-CSP (Zinsmaier et al., 1994), and anti-Syx at 1:20 and rabbit antisynaptotagmin (Littleton et al., 1998) at 1:500. All the fluorescently conjugated secondary antibodies were raised in donkey and obtained from Jackson Research Labs, Inc. (USA).

dsRNA Treatments

dsRNA treatments were performed as per the protocols described by Eaton et al. (2002). In brief, approximately 600 bp long double stranded DNA fragments were PCR amplified from the fly genomic DNA by using primers specific to KLP64D, KLP68D, and DmKAP (Table 1). A 26 base pair T7 promoter element (5′-TAATACGACTCACTATAGGGAGACCAC-3′) was attached to the 5′ ends of both the forward and reverse primers. The double stranded RNA fragments were then generated from the PCR amplified DNA by using the superscript T7 RNA polymerase kit (Roche Diagnostics GmbH). dsGFP was prepared from a bacterial plasmid containing the GFP coding sequence. Embryos were collected after 30 min of egg laying, incubated for 16 h at RT, and then soaked for 24 h in 1% sucrose solutions containing 5 m*M* dsRNA. The larvae hatched during this period were transferred to fresh vials and grown until the late third instar stage (84–90 h AEL), then dissected and stained using the protocol as described above.

Table 1 Primers for PCR Amplification of Specific DNA Fragments, Used for dsRNA Preparation

Gene	T7+Forward (5′–3′)	T7+Reverse (5′–3′)	Position (cDNA)
Klp64D	GAAAAGGAGGAACTGGCC	TCGCCTGGCAGTCGTCGG	1302–2031
Klp68D	GAGCTCGAGATGGCTCAG	TTTGTTGACCAGGCCGCG	1680–2355
DmKAP	CTGATCAAGAGTCAGATCC	CGTTTGCGTGAACATGCC	1021–1664
GFP	ATGGTGAGCAAGGGCGAG	TTACTTGTACAGCTCGTC	0–720
	T7 promoter sequence-5′-TAATACGACTCACTATAGGGAGACCAC-3′		

Drug Treatments of Larval Brain

Embryos were collected after 2 h of egg laying and aged until 72 or 90 h in a 25°C incubator. After this, the larval brains were dissected in Schneider's Drosophila Media (GIBCO BRL, Invitrogen Corp., USA) containing inactivated FCS (Sigma Chemicals Co. USA), transferred to a fresh drop of the same media containing either 0.03% DMSO, 5 μM vinblastine (dissolved in DMSO), or 5 μM colchicine, and incubated at room temperature or at 15°C for a predetermined period. Then they were fixed and immunostained as described above.

Image Analysis

For the measurement of AT index of different presynaptic antigens, the brains of precisely aged larvae were dissected and processed together in a single batch, as per the above descriptions. The last six abdominal segments of the ventral ganglion were imaged from all the specimens for the ratiometric estimation. Multiple optical sections were collected using a 40X/NA 1.3 oil objective (Nikon Corp., Japan), which was fitted in a Nikon eclipse TE300 inverted microscope, and through a Radiance 2100 LSCM scan head. To avoid over sampling, the Z-step was set to 1 μm and every alternate section of an image stack was selected for measurement. The system was automated by using a macro in ImageJ (http://rsb.info.nih.gov/ij) to randomly place a 25 × 25-pixel box in the selected region of the image and the mean intensity levels were measured in an 8-bit scale (0–255 levels). The average of many such measurements from an entire brain specimen was estimated as a single data point.

Disruption of anterograde AT is expected to increase the average staining intensity, I_C [Fig. 2(A)], due to excessive retention of the antigen in the cell body and axons. A simultaneous disruption of the retrograde transport would not change the I_N [Fig. 2(A)]; in some cases, however, it may decrease due to normal degradation. As a result, the $I_N - I_C$ would reduce even further whereas the $I_N + I_C$ would remain unaltered, or increased to a certain extent. Therefore, to compare differences amongst different specimens, a normalized AT index was estimated for each specimen using the formula $(I_N - I_C)/(I_N + I_C)$. In addition, the I_N and I_C values of certain antigens could be altered by selective turnover and/or synthesis defects, and this would also alter the AT index. The average AT indices with error bars depicting ±SD were plotted, and significance between two data sets was calculated according to the Mann-Whitney two-tailed tests of significance and by using the GraphPad InStat V3.05 (GraphPad Software Inc.) data analysis package.

Immunoprecipitation Assay

About 50 isolated fly heads were homogenized on ice in 150 μL lysis buffer containing 20 mM HEPES (pH 7.4), 150 mM NaCL, 5 mM $MgSO_4$, 5 mM EGTA, 1 mM PMSF, and protease inhibitor cocktail and centrifuged at 13,000×g for 30 min. The supernatant was incubated with appropriate antiserum (1/10 vol) for 1 h and then for another hour with 30 μL of proteinA sepharose beads on a rocker. The beads were washed with large volumes of lysis buffer, boiled in sample loading buffer, and then the extracts were separated by 10% SDS PAGE, transferred to PVDF membrane, and probed by different antisera. Westerns were developed by using ECL chemiluminescence detection kit (GE Healthcare Ltd.). The KLP64D and DmKAP specific antisera were raised by immunizing female rats with purified GST-KLP64D stalk-tail and GST-DmKAPN400 fragments, respectively. Specificity and titer of these antisera were tested by ELISA against the purified KLP64D stalk-tail and N-400 fragment of DmKAP, respectively.

RESULTS

Drosophila brain develops from a fixed set of primary glia and neuronal lineages generated from the stem-cell-like divisions of neuroblasts. The first wave of neuroblast proliferation occurs at the early embryonic stages and this leads to the formation of larval brain [Fig. 1(A)]. After a phase of mitotic dormancy, neuroblasts become active again at the first instar larva stage and give rise to a second set of neuronal and glial lineages, which makes the adult ganglion during metamorphosis (Truman and Bate, 1988; Ito and Hotta, 1992). The neuroblast proliferation and differentiation generates a concentrically organized ganglionic brain [Fig. 1(B,C)], comprised of a central neuropil formed by neuronal processes and synapses, surrounded by an outer cortex of neuronal and glial cell bodies (Strausfeld, 1976). The cortical as well as the sensory neurons project to the ventral neuropil in a segment-specific manner [Fig. 1(C)].

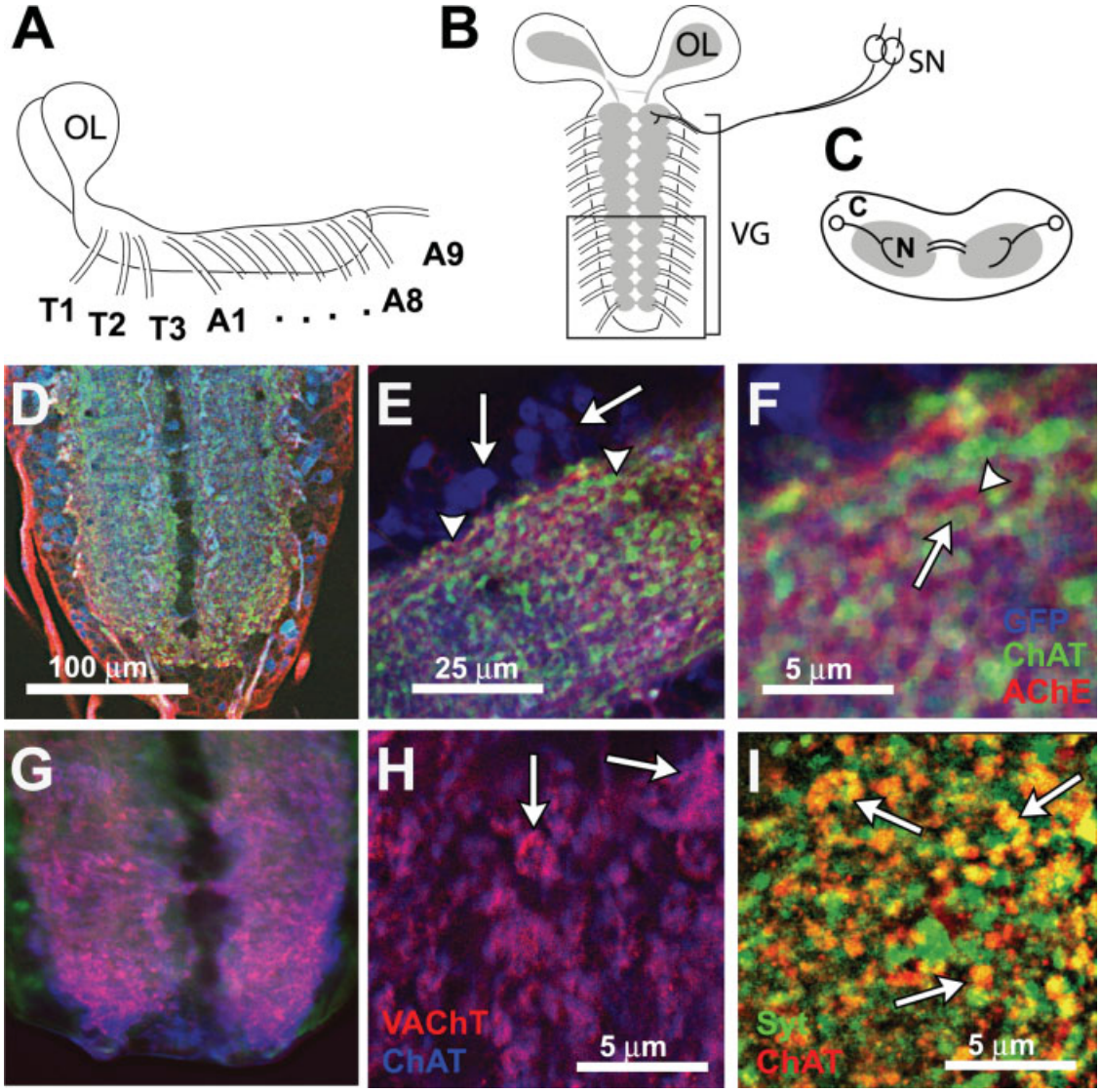

Figure 1 Localization of ChAT, AChE, and other presynaptic antigens in larval ventral ganglion and segmental nerve axons. (A–C) Schematic representation of the lateral (A) and dorsal (B) views of a larval brain. Grey area indicates the neuropil, which contains neurites and synapses. Ventral ganglion (VG) is laterally symmetric, which receives afferent axonal projections from sensory neurons (B) and from the cortical neurons of the brain (C). Box in (B) indicates the area used for this study. (D–F) ChAT (green) and AChE (red) localization in wild-type VG shown at different magnifications as indicated by scale bars on the figures. Cholinergic neurons, marked by cytoplasmic GFP expression, are shown in blue. (E) The arrow indicates a cholinergic cell body at the cortex and the arrowhead indicates synaptic bulbs at the neuropil. (F) ChAT (arrow) and AChE (arrowhead) localization at a typical presynaptic bulb. (G,H) ChAT (blue) and VAChT (red) colocalize at the synaptic bulbs (arrows) in VG. (I) ChAT (green) also colocalizes with synaptotagmin (Syt, red) at the synaptic terminals.

The morphological and functional differentiation of the secondary neurons is delayed (Truman, 1990). Though the axonal processes of these neurons penetrate the cortex, they halt at the cortex-neuropil border until the beginning of metamorphosis (Truman et al., 1994). However, the neuropil volume increases after every molt, indicating that the existing processes increase their arborization during this period. The overall neuropil volume and synaptic density in the thoracic and abdominal segments of the ventral gan-

glion remain unchanged during the third larval instar between 72 and 96 h after egg laying (AEL). Therefore, we chose this period for our analysis.

ChAT, AChE, and VAChT are expressed in the same presynaptic neuron in *Drosophila* (Zador and Budai, 1994; Kitamoto et al., 2000). Immunostaining wild-type larval brain revealed that most of the ChAT and AChE antigens localize in the neuropil region [Fig. 1(D,E)] at the third instar stage. Further analysis revealed that these two antigens are enriched in mutually exclusive domains at the neuropil [Fig. 1(F)]. On the other hand, the VAChT antigen colocalized with ChAT within the presynaptic bulbs [arrows, Fig. 1(H)]. ChAT staining in the presynaptic bulbs also overlapped with that of synaptotagmin [arrows, Fig. 1(I)] and cystein string protein (CSP) (data not shown), indicating that these two antigens are also present in the presynaptic compartments of cholinergic neurons.

Anterograde Transports of ChAT and AChE Require Microtubules

To assess the role of microtubules in the AT of ChAT and AChE in *Drosophila*, we treated isolated larval brain with microtubule destabilizing agents in tissue culture media. Previous studies showed that treatments with low dosage of vinblastine affect the microtubule-dependent ATs in isolated neurons (Francis et al., 2005). In addition, colchicine treatment was shown to block anterograde transport of ChAT in *Aplysia* neurons (Koike et al., 1989) and AChE-containing vesicles were found to associate with microtubules in the axons of mammalian neurons (Kasa, 1968).

Increased accumulations of ChAT and AChE were observed within 2 h of 5 μM vinblastine [arrows, Fig. 2(B,E)] and 5 μM colchicine [arrows, Fig. 2(C,F)] treatments, respectively. These were found in the cortical region as well as at the margins of the neuropil, which is largely populated by neurites (arrowheads, Fig. 2). The control specimens, treated with 0.03% DMSO, showed no such defect. The cortical accumulations of both ChAT and AChE progressively increased with the treatment time [Fig. 2(G)]. Interestingly, the AChE accumulations occurred at a rate faster than that of ChAT. This was more prominent in the 72 h AEL brain specimens [Fig. 2(H)], in which AChE accumulated in the axons [arrows, Fig. 2(H)] and cortex [arrowheads, Fig. 2(H)] before ChAT did. This suggests that microtubule-dependent transports play an important role in synaptic localizations of ChAT and AChE in *Drosophila* and the latter is perhaps transported at a faster rate.

Quantification of ChAT and AChE Transports in the Larval Brain

To establish further the inherent difference in the transports of ChAT and AChE, we designed a quantification technique to arrive at an AT index from the immunostained specimens [Fig. 3(A)]. It was designed to highlight changes in the neuropil levels of an antigen with respect to the cortex. For instance, accumulation of an antigen in the cortex due to abnormal transport as well as its depletion from the neuropil/cortex due to altered stability or a lack of transport would reduce the AT index. In addition, a net rise in the neuropil levels of an antigen due to increased anterograde transport would increase the index. A constitutive turnover of an antigen would not alter the index. However, the conjugated changes in the neuropil and cortical levels, as it may happen due to disruptions in the AT, would produce relatively higher differences in the AT indices.

The AT indices of ChAT and AChE were altered significantly within 2 h of both the vinblastine and colchicine treatments [Fig. 3(B)]. However, with respect to the DMSO control, the level of AT_{AChE} reduction was about two-fold more than that of AT_{ChAT}, indicating that the two antigens could be transported at different rates. The possibility that such changes occurred due to retractions of cholinergic neurites from the neuropil was ruled out by measuring the AT_{GFP} values from the *ChaGal4 UAS-GFP* larvae [Fig. 3(B)], which were not significantly altered after the drug treatments. Expression of cytoplasmic GFP in the cholinergic neurons of these larvae marked the cell bodies and neurites. Hence, a possible retraction of neurites from neuropil after the drug treatments would have reduced the AT_{GFP} value.

Differential Transports of ChAT and AChE during Third Instar Larva Stage

In *Drosophila*, ChAT mRNA is expressed for brief durations during the first instar larva and the pupa stage, and the enzyme activity was observed to peak at 72 h AEL (Carbini et al., 1990). Therefore, it is likely that a brief pulse of ChAT transport may take place just preceding metamorphosis. Systematic measurement of AT indices revealed that indeed the AT_{ChAT} values increase steadily between 72 and 90 h AEL [Fig. 3(C)], which confirmed that a net anterograde flow of ChAT occurs during this period. In contrast, AT_{AChE} remained unaltered throughout this period [Fig. 3(C)]. Previous analysis suggested that AChE is transported bidirectionally at a faster rate

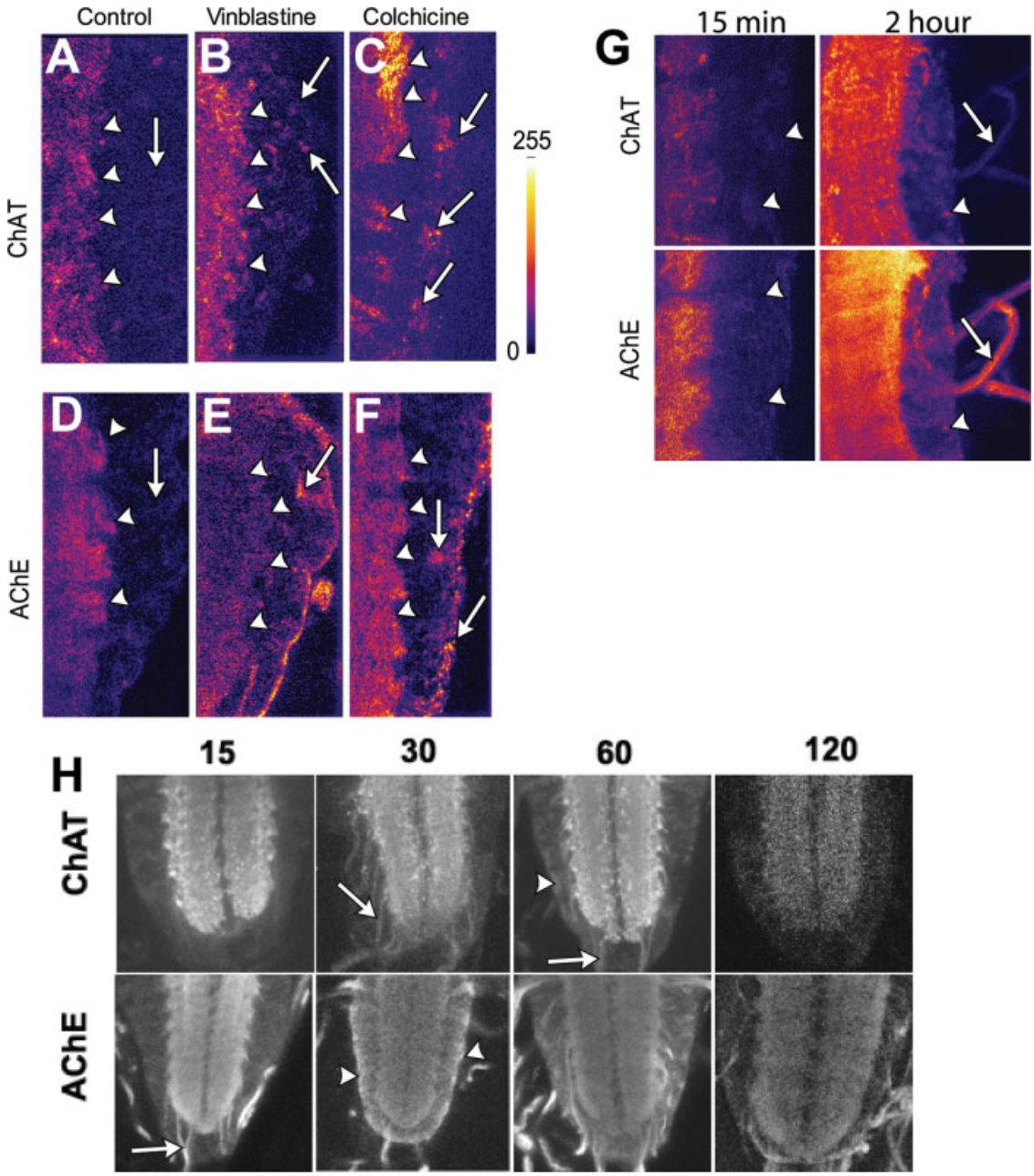

Figure 2 ChAT and AChE localization profiles in the larval brains after vinblastine and colchicine treatments. (A–F) A part of the ventral ganglion stained with ChAT (A–C) and AChE (D–F) antisera, respectively, after a 2 h treatment with 0.3% DMSO (A,D) as control, 5 μM vinblastine (B,E), and 5 μM colchicine (C, F), respectively. Gray levels (0–255) in individual pictures are depicted in a false color scale as indicated at the right margin. Arrows indicate neuronal cell bodies and arrowheads mark the boundary between the neuropil and cortex in all figures. (G) ChAT and AChE accumulation in 90 h AEL larval brain after 5 μM vinblastine treatments of 15 min and 2 h durations, respectively. Arrows indicate the segmental nerve, and the arrowheads indicate a neuronal cell body at the cortex. (H) Ventral ganglia from 72 h AEL larvae stained with ChAT and AChE antisera, respectively, after different periods of colchicine treatments as indicated at the top of each column. Arrowheads indicate neuronal cell bodies and arrows mark the ectopic accumulation of the antigens in axons. Note that AChE accumulates in the neuropil-cortex boundary as well as in the segmental nerve before that of ChAT. [Color figure can be viewed in the online issue, which is available at www.interscience.wiley.com.]

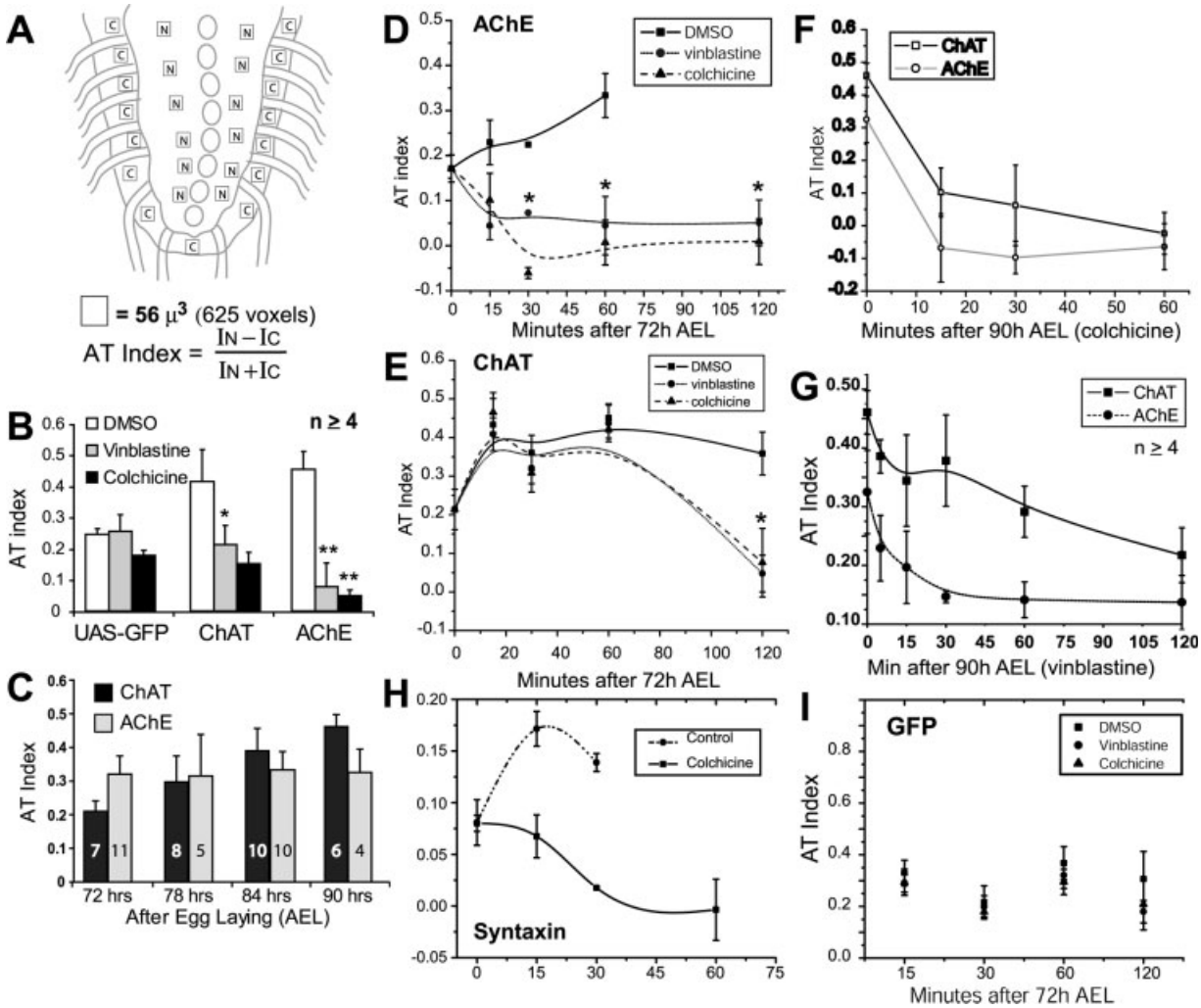

Figure 3 Axonal transport profiles of ChAT, AChE, and other presynaptic antigens. (A) Schematic of the larval VG shows the positions of the sampling boxes. Mean intensity of staining was calculated by randomly selecting 25 × 25 pixel area in the neuropil (marked N) and the cortical regions (marked C) of the last five abdominal segments. It covered approximately 56 cubic μm volume in the specimen. (B) AT indices for GFP, ChAT, and AChE are calculated after 2 h of DMSO (open bars), vinblastine (grey bars), and colchicine (solid bars) treatments, respectively. (C) AT_{ChAT} (solid bars) and AT_{AChE} (grey bars) variations during 72–90 h AEL period. (D,E) AT_{AChE} (D) and AT_{ChAT} (E) levels after different periods of DMSO (control), 5 μM vinblastine, and 5 μM colchicine treatments, respectively, of isolated 72 h AEL larval brains. (F) AT_{ChAT} and AT_{AChE} profiles from 90 h AEL specimens after different durations of 5 μM colchicine treatments. (G) Similar measurements were done after 5 μM vinblastine treatments of 90 h AEL specimens at 15°C. (H) The AT_{Syx} changes due to 5 μM colchicine treatments. (I) AT_{GFP} levels after a similar set of treatments as indicated in (D) and (E). Significance levels were tested with respect to the wild-type values using two-tailed Mann-Whitney nonparametric test. Significant ($*p < 0.01$), very significant ($**p < 0.001$) and not so significant (ns) differences are indicated on top of each bar or dot plots. For all plots, error bars indicate ±SD and n values are indicated on each bar. For the data presented in (D,E,F), the n values were ≥4. The actual significance values for the plots in (D) and (E) are presented in Supplementary Table 1.

than ChAT. A typical fast AT occurs at an average rate of 0.1–2 μm/s. At this rate, it will only take a few seconds to cover the distance between the cortex and neuropil. Because measurements were done at every 6 h, they would not reveal transient changes in the AChE levels. Nevertheless, this result suggested two

distinct profiles of ChAT and AChE transports in the larval neurons.

To assess this, we recorded the AT index variation due to different extents of the drug treatments with specimens isolated from 72 h AEL larvae. We found that extended periods of DMSO treatment selectively extract AChE from the cortex and improve antibody penetration into the tissue. As a result, the AT_{AChE} was progressively increased with the time of treatment [Fig. 3(D)] while the AT_{ChAT} was enhanced at all time points [Fig. 3(E)]. However, with colchicine or vinblastine in the media, the AT_{AChE} were rapidly reduced during the first 30 min and then stabilized [Fig. 3(D)], but the AT_{ChAT} was only significantly reduced after 2 h [Fig. 3(E)]. This suggested that AChE is transported at a rapid rate even at 72 h AEL, and the ChAT transport probably starts from 73 h AEL. Interestingly, the proportional reduction of AT_{AChE} within 1 h of the drug treatments was similar to that of AT_{ChAT} reduction between 72 + 1 h and 72 + 2 h AEL, indicating that the rates at which these two are transported would be similar.

This was tested further by measuring AT indices from the 90 h AEL brains. This revealed an almost similar rate of decay for both AT_{AChE} and AT_{ChAT} during the first 30 min [Fig. 3(F)], although the AT_{AChE} appeared to equilibrate by 60 min while the AT_{ChAT} appeared to decay at a slower rate. This difference became clearer when the same experiment was performed at 15°C [Fig. 3(G)]. These results suggest that at the peak of the ChAT transporting period, both the ChAT and AChE are transported at similar rates. It also established that AChE is constitutively transported at a constant rate throughout the larval stage. The difference in the rates only becomes apparent when the accumulation is integrated for longer durations as depicted in Fig. 3(B) above. Furthermore, the AT_{AChE} curves equilibrated faster than the AT_{ChAT} curve. This probably happened due to selective extraction of the antigen by DMSO in the media. Alternatively, it could also be contributed to by a rapid turnover of accumulating AChE in the cell body. The current assay is inadequate to distinguish between these two possibilities.

In addition, we found that treatments with microtubule-destabilizing agents also changed the AT indices of syntaxin [Syx; Fig. 3(H)], in a manner different from that of AT_{ChAT} and AT_{AChE}. The AT_{GFP}, however, showed no such changes with time [Fig. 3(I)]. Syx is known to be transported along with VAMP and other t-SNARE complex proteins in the axons in a microtubule-dependent manner (Shiff and Morel, 1997; Ahmari et al., 2000). Altogether, this established that treatment with low doses of microtubule-destabilizing agents affects the microtubule-dependent transport of proteins in the axons, and though both ChAT and AChE are transported at a similar rate, their profiles are different.

ChAT and AChE Accumulate in Neuronal Cell Bodies and Axons in *Klp64D* Larvae

Mutation in *Klp64D* was shown to increase the accumulation of ChAT in the segmental nerve axons (Ray et al., 1999). We further found that in *Klp64D* homozygous larvae (both *k1* and *k5* alleles), the AChE staining was reduced at the neuropil [Fig. 4(A)] and appeared in the cell bodies [arrowheads, Fig. 4(B)] and neurites [arrow, Fig. 4(C)]. It was present in punctate structures at the cell bodies of the sensory neurons [Fig. 4(E)]. However, most of the ChAT- [arrow, Fig. 4(E)] and AChE- [arrowhead, Fig. 4(E)] positive punctae did not overlap. In addition, these antigens were present in the segmental nerve axons [arrows, Fig. 4(G)]. We also found that the AChE staining was increased along the segmental nerve, but the pattern of accumulation was different from that of ChAT [Fig. 4(G)]. Altogether, these observations indicate that *KLP64D* is required for the synaptic localization of AChE as well.

siRNA-Mediated Knock-Out of *KLP64D*, *KLP68D*, and *DmKAP* Causes Selective Accumulation of ChAT and AChE in the Cell Bodies and Axons

To further ascertain the roles of other kinesin-2 subunits in their transport, we used a specific siRNA-mediated knock-out technique to eliminate *Klp64D*, *Klp68D,* and *DmKap* mRNAs, and studied ChAT and AChE accumulations in these backgrounds at the larval stages. Feeding early first instar larvae with specific dsRNA fragments causes selective degradation of the corresponding mRNA, which in turn reduces the respective enzyme/protein activity in the tissue (Eaton et al., 2002).

The *Klp64D* -specific dsRNA produced strong accumulation of ChAT and AChE antigens in axons [arrowheads, Fig. 5(B,E)]. Similar accumulations were observed after *dsKlp68D* feeding as well [arrowheads, Fig. 5(C,F)]. Here again, we noticed that the accumulating ChAT- and AChE-positive punctae in the cortical cells of the VG and in the segmental nerve axons did not overlap (Supplemental Fig. 1). The *dsKap* treatment also caused accumulation of ChAT [Fig. 5(G,H)] and AChE (not shown) in the cell bodies and neurites, but not CSP [Fig. 5(I,J)].

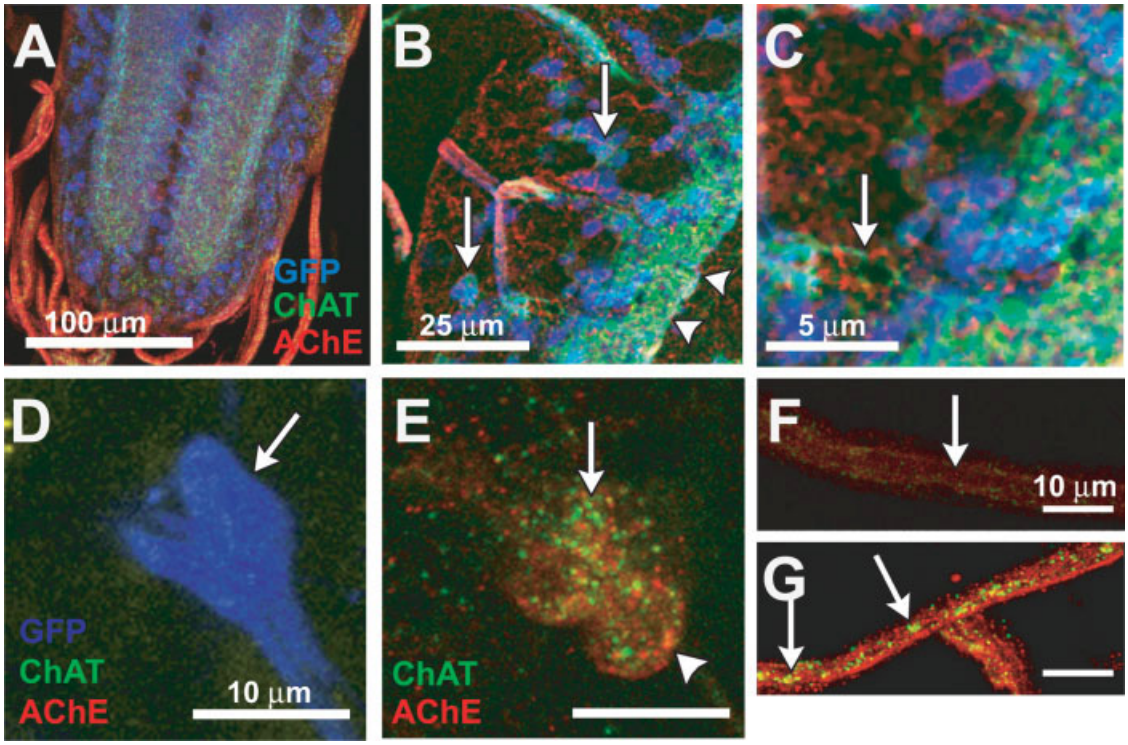

Figure 4 ChAT and AChE localizations in the VG of *Klp64D*^{k5} homozygous larva shown at different magnifications as indicated in the figures. (A,B) Arrows indicate cell bodies and arrowheads indicate the neuropil margin. (C) Arrow indicates a ChAT- accumulating neurite. (D,E) ChAT (green) and AChE (red) localization at the cell body of sensory neurons innervating the lateral chordotonal organ (lch5) in wild-type (D) and *Klp64D*^{k5} (E) homozygous larva. Cholinergic neurons are marked by the GFP expression (blue). (D) Sensory neuron cells from a wild-type larva (arrow) showing no ChAT or AChE accumulations. (E) ChAT (arrow) and AChE (arrowhead) accumulations in the neuronal cell bodies in *Klp64D*^{k5} larva. (F,G) ChAT (green) and AChE (red) localizations in the segmental nerve axons from wild-type (F) and *Klp64D*^{k5} (G) larvae. Arrows indicate the segmental nerve.

As expected, *dsGFP*, as well as the buffer alone, did not produce such abnormal accumulations. Altogether, these data indicated that in addition to KLP64D, the KLP68D and DmKAP subunits are also involved in ChAT transport to the synapse and possibly that of AChE as well. However, the data did not rule out the possibility of such a defect arising as the secondary effect of the ChAT transport block in these specimens.

Mutations in Klp64D Independently Affect ChAT and AChE Transports

Because the drug treatment data suggested that ChAT and AChE have different transport profiles, we wanted to establish whether KLP64D would be independently required for both the AChE and ChAT transports. For this, we measured the AT_{AChE} and the AT_{ChAT} values from *Klp64D* homozygous larvae at 72 and 90 h AEL, respectively (Fig. 6). We observed significant reduction of AT_{ChAT} only at 90 h AEL [Fig. 6(A)] in *Klp64D* larvae. In contrast, the AT_{AChE} values were reduced significantly at both 72 and 90h AEL [Fig. 6(B)] in these specimens. These two sets of data showed that loss of KLP64D activity independently affects the two events. Expectedly, both of the defects were rescued by *UAS-Klp64D* in the mutant backgrounds, which firmly mapped the phenotypes to the loss of KLP64D activity in these mutants. The AT_{CSP} and AT_{Syt} remained unaltered in *Klp64D* larvae at both 72 and 90 h AEL [Fig. 6(C,D)] and similar results were obtained with the Syx-specific antisera as well (not shown). This indicated that KLP64D is not required for the transport of these latter antigens. However, it is still formally possible that altered neurite morphology of cholinergic neurons could cause such a change in the AT index in mutants. We ruled out this possibility because AT_{GFP} remained unchanged at both 72 and 90 h AEL

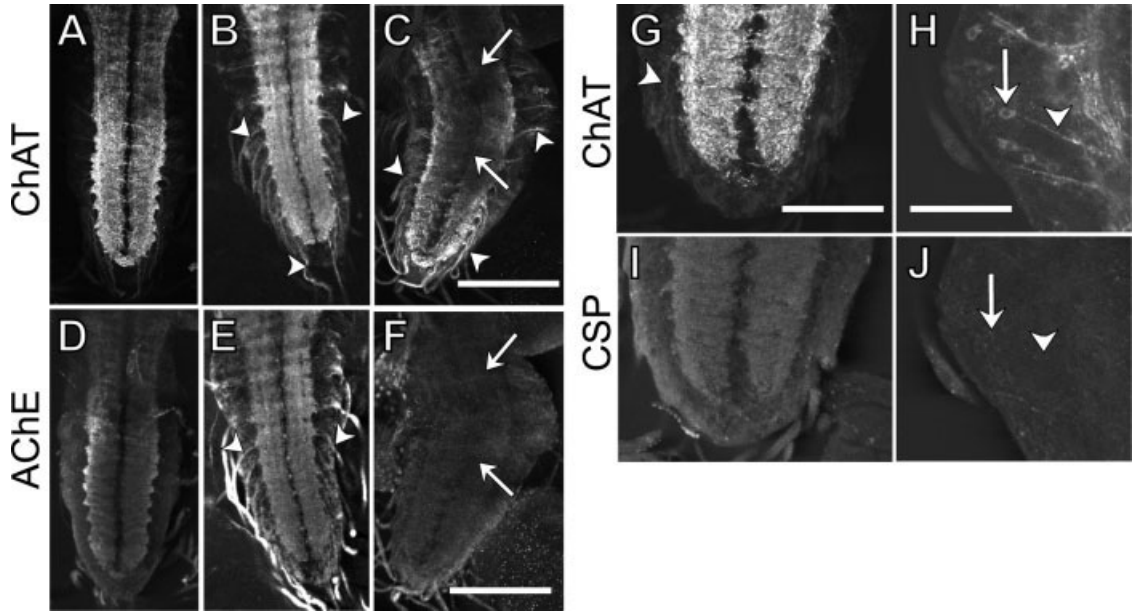

Figure 5 Effects of kinesin-2-subunit specific dsRNA treatments on ChAT and AChE localizations in the ventral ganglion. ChAT (A–C) and AChE (D–F) staining in the VGs from dsGFP (A,D), dsKlp64D (B,E), and dsKlp68D (C,F) fed larvae. Arrows indicate neuropil region and arrowheads the segmental nerve axons in different figures. Note that ChAT and AChE are accumulated in axons in dsKlp4D- and dsKlp68D-treated larvae. dsKlp68D treatment also reduced the ChAT (C) and AChE (F) staining from the neuropil region. (G,H) VG from dsDmKap-treated larva and stained with anti-ChAT. (H) Cortical neurons show ChAT accumulation in the cell body (arrow) and neurite (arrowhead). (I,J) The same region stained with CSP antiserum showed no such accumulations. Scale bar in (C) and (F) indicates 100 μm for figures (A–F), in (G) it indicates 50 μm for (G) and (I), and in (H) it indicates 25 μm.

[Fig. 6(E)] in the *ChaGAL4 UAS-GFP, Klp64D*^{k1} homozygous larvae. Hence, this confirmed that KLP64D is selectively and separately required for the AT of AChE and ChAT. Similar reductions of AT_{ChAT} and AT_{AChE} were observed in the homozygous *DmKap* larvae as well (data not shown). This further implicated the accessory subunit of kinesin-2 in these two processes.

ChAT and AChE Associate with Kinesin-2 in Cell-Free Extracts

One of the essential requirements of AT is that the motor complex should physically associate with the cargo. In order to establish such an association between AChE, ChAT, and kinesin-2, we analyzed the immunoprecipitation profiles of AChE and ChAT by kinesin-2-specific antisera and vice versa. Amongst the several different bands stained by the polyclonal AChE antiserum, only the ≈80 kDa isoform was precipitated by the antibodies specific to KLP64D, KLP68D, and DmKAP subunits [Fig. 7(A)], while both the ChAT and Syx antisera failed to precipitate any AChE reactive polypeptides [Fig. 7(A)]. MAb4B10, which stained the neuropil in larval brain like AChE, also failed to pull down AChE and KLP68D [Fig. 7(A)]. All these established the specificity of the immuno-precipitation reactions. As expected, the AChE antisera also precipitated the KLP64D, KLP68D, and DmKAP [Fig. 7(A)]. Altogether, this suggested that AChE could associate with kinesin-2 subunits in neurons but it is unlikely to associate with ChAT.

The ChAT antiserum also pulled down the 82 kDa KLP68D and a ≈100 kDa DmKAP band [Fig. 7(A)]. Interestingly, we observed an improved efficiency of the IP by supplementing the lysis buffer with 10 nm Taxol and 1 m*M* ATP. Under this condition, the purified KLP68D antiserum [Fig. 7(B)] recognized an 82 kDa (the expected size of KLP68D) and a ≈120 kDa band in the adult head extracts and predominantly the higher mobility band in the abdominal extracts [Fig. 7(B)]. It also coprecipitated ChAT along with these two bands [Fig. 7(B)]. In addition, the KIF3A-specific antisera pulled down the 120 kDa

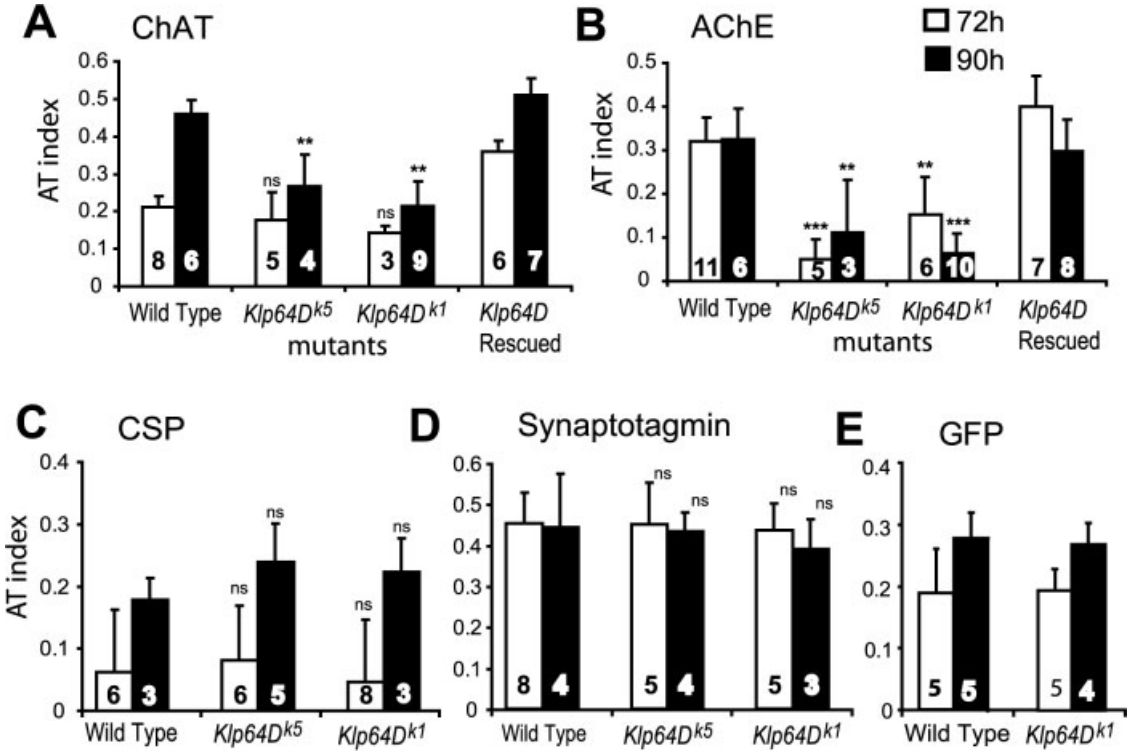

Figure 6 AT indices for ChAT, AChE, and various other presynaptic antigens at 72 and 90 h AEL from wild-type and *Klp64D* larvae. The indices are calculated and plotted as described in Figure 3. Significance levels were tested with respect to the wild-type values using two-tailed Mann-Whitney nonparametric test. Very significant (**$p < 0.001$), extremely significant (***$p < 0.0001$), and not so significant (ns) differences are indicated on top of each bar. For all plots, error bars indicate ± SD and *n* values are indicated on each bar.

KLP68D band as well as ChAT from the head extracts of flies expressing the transgenic UAS-KIF3A in the nervous system [Fig. 7(B)]. As of now, we are unable to ascertain the identity of the higher band, which could be either a modified KLP68D or yet another isoform of the protein. Together, these experiments indicated that ChAT associates with the kinesin-2 subunits in neurons. However, ChAT and AChE are unlikely to associate with each other.

DISCUSSION

We have described a novel assay utilizing the quantitative immunofluorescence measurement to detect minute changes in the asymmetric distribution of synaptic antigens due to abnormal ATs. We used microtubule destabilizing drugs at low concentration to derail the intracellular transport and showed that this causes accumulation of ChAT and AChE antigens in the cell body region at dissimilar pattern. In addition, the siRNA mediated knock-out experiment and genetic analysis suggested that all the three known subunits of kinesin-2 in *Drosophila* are involved in transporting these two antigens. The AT index measurements in homozygous *Klp64D* mutants showed that loss of the protein reduces both the AT_{AChE} and AT_{ChAT} at two different time points, indicating that KLP64D separately transports these two enzymes. Finally, the immunoprecipitation results confirmed that both AChE and ChAT separately associate with kinesin-2 in the nervous tissue.

Previous studies using sucrose density gradient centrifugation analysis of axonal extracts from mouse brain showed that KIF3A is predominantly partitioned in the denser fraction (Kondo et al., 1994), and a similar study in our laboratory cofractionated the KLP64D, KLP68D, and DmKAP along with the 72 kDa ChAT in the 16–20 S range (D. Harinath and K. Ray, unpublished data). This further supports that kinesin-2 could associate with AChE and ChAT in the axons. Together, these data indicate that AChE and ChAT are differentially transported by kinesin-2 in *Drosophila*.

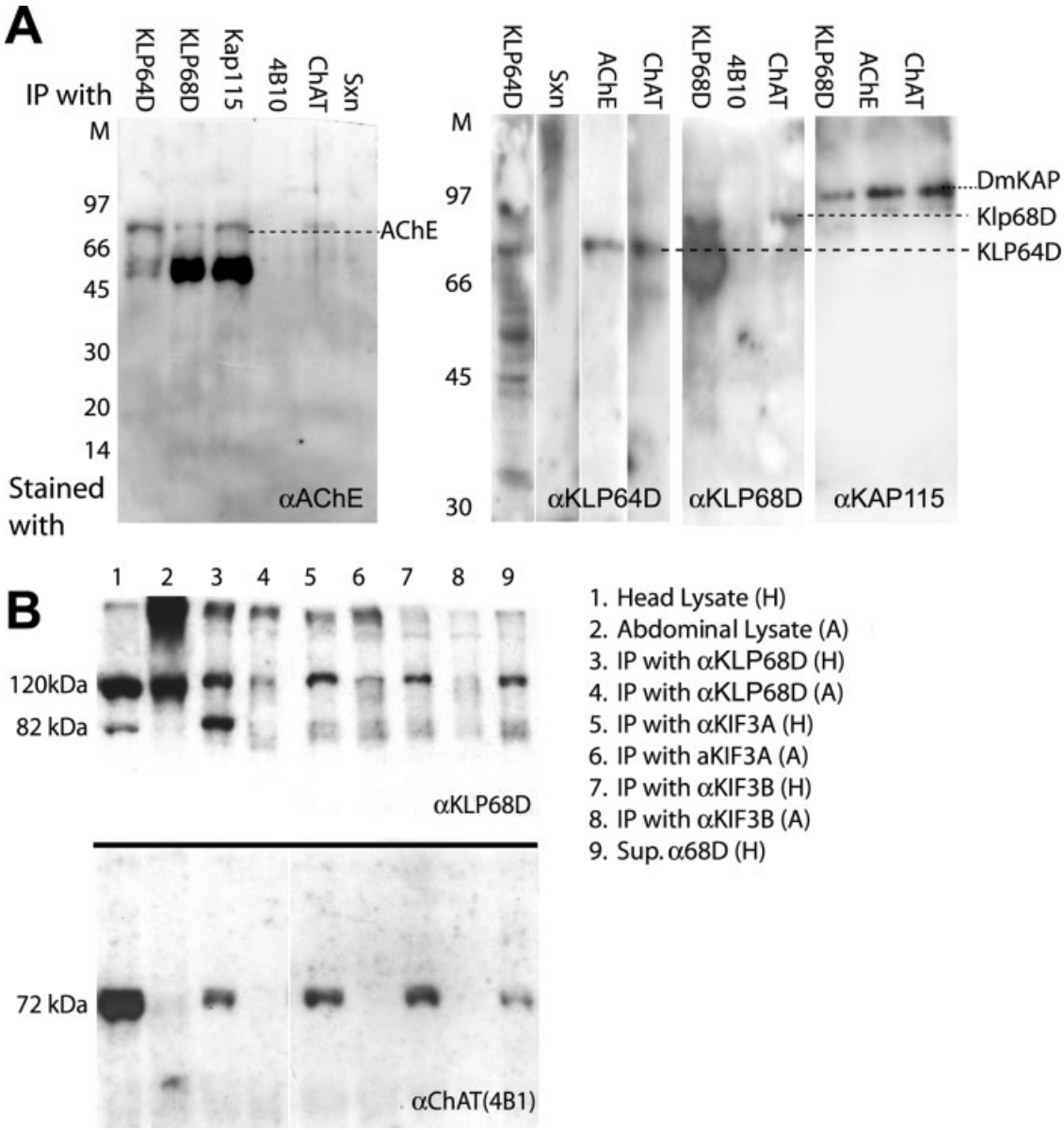

Figure 7 Immunoprecipitation of ChAT and AChE by kinesin-2 subunit specific antisera. (A) Western blots of different immunoprecipitation reactions, as indicated at the top margin of each lane, were stained with AChE-, KLP64D-, KLP68D-, and SpKAP115-specific antisera, as indicated on the bottom right margin of respective blots. (B) IP experiments were also performed with the adult head (H) and abdominal (A) extracts from flies expressing mouse KIF3A in the neurons from a transgene. It shows that ChAT could associate with KIF3A as well.

Kinesin-2 and the Mechanism of Anterograde ATs of Acetylcholine Synthesis and Recycling Enzymes

Previous studies have shown that AChE is transported rapidly in a bidirectional fashion in rat sciatic nerve axons (Wooten and Cheng, 1980) and in other peripheral neurons (Torres et al., 1983). The fastest rate was observed for a tetrameric (G4) form of AChE, which is incorporated in an 11–20S complex. However, the majority of the experiments in the past indicated that ChAT is transported anterogradely at a rate 10-fold slower than that of AChE (Wooten and Cheng, 1980; Tucek, 1975). All these studies were done by estimating the accumulated enzyme activity at the sciatic nerve ligature after a period of 24 h. Measuring in a shorter time window of several minutes and by using the immunofluorescence quantification assay, we show

that the transports of these two antigens occur at marginally different rates in *Drosophila*. However, it was more interesting to find that ChAT and AChE are transported in two different profiles.

How could kinesin-2 transport cargoes at two apparently distinct profiles? We demonstrated that loss of kinesin-2 causes ChAT and AChE accumulations in separate punctae in the neuronal cell bodies and axons, which implies that these two are packaged separately. It was confirmed further by the immunoprecipitation analysis. Therefore, ChAT and AChE could interact with kinesin-2 through independent sites present on one or more subunits. Alternatively, both of them could interact through the same site and their loading onto the motor could be regulated by the relative abundance of AChE and ChAT in the cell. Although its speed in the axons is yet to be determined, the particles associated with kinesin-2 move at a rate similar to that of the fast ATs in the sensory cilia (Snow et al., 2004). Hence, individual motor complexes containing either AChE or ChAT may actually move at the same rate, but a relatively higher frequency of AChE-containing complexes in the axons would result in an apparently faster AChE transport rate. Kinesin-1 is also known to associate with JIP and GRIP1 complexes through KLC and KHC, respectively, and transport them towards the pre- and postsynaptic compartments (Bowman et al., 2000; Verhey et al., 2001; Setou et al., 2002). However, these were observed in different types of neurons and the rates of the respective transports were not determined.

The average speed of axonal transport of a cargo is also determined by the time it actually spends moving in the axons, which is the duty ratio. Most of the vesicular cargoes move in the axon with the higher duty ratio, which results in a faster average speed, while the soluble proteins like microtubule and neurofilaments (NF) have a lesser duty ratio (Brown, 2003, for review). It was recently shown that the so-called slow rates of transport of microtubule and NF are actually caused by rapid but intermittent and asynchronous movement of these in the axons (Wang et al., 2000; Roy et al., 2000; Wang and Brown, 2001, 2002). Microtubule-dependent fast axonal motors play an important role in all these transports (Xia et al., 2003; He et al., 2005).

The rates of ChAT and AChE accumulations are similar at the pick of the ChAT transporting period, beginning at ~73 h AEL. But there is negligible transport of ChAT before that. This suggests that the AChE:kinesin-2 and the ChAT:kinesin-2 complexes would have a similar duty ratio in axons. Thus, the apparently slower rates of ChAT transport could occur due to intermittent and less frequent transport of this protein. This may imply that the availability of cargoes controls the transports. This is an interesting possibility, which could be resolved by direct analysis of ChAT transport in live neurons.

Balancing ChAT and AChE at the Synapse by Kinesin-2-Dependent Anterograde Transport

Though it is still unclear how different sets of intracellular transports are regulated, some experimental evidence indicates that proteins involved in a single biochemical process are likely to be packaged together and transported by a specific motor. For instance, the enzymes of JUN kinase signaling cascade are assembled in a scaffold and transported by conventional kinesin motors in axons (Bowman et al., 2000; Verhey et al., 2001), which interact with the JIP/SYD subunit of the scaffold. Similarly, proteins involved in synaptic vesicle docking, for example, synaptotagmin, synaptophysin, and Rab3A, and so forth, are transported together in the axon in a prefabricated organelle by an anterograde microtubule-dependent motor protein (Ahmari et al., 2000; Yonekawa et al., 1998; Okada et al., 1995). It is also known that VAMP and t-SNARE are associated with each other even before they enter the axons (Shiff and Morel, 1997). All of this indicates the assembly of functionally related enzymes in a scaffold or organelle before they are transported into the axon. This perhaps helps to maintain their relative stoichiometry at the synapse.

ChAT and AChE have distinctly different turnover rates in the mammalian axons (Lubinska et al., 1964; Fonnum et al., 1973). Maintaining their proportional balance at the synapse would require careful regulations of the AT rates. Hence, a natural hypothesis would be to assume that different motors would transport these two proteins in the axon. Our results suggest that ChAT and AChE are also differentially transported in the axons in *Drosophila*. However, quite surprisingly, we find that both are transported by kinesin-2. Because temporal patterns of ChAT and AChE expression are different and our results show that the ChAT transport follows its expression pattern, suggesting that actual regulation of such transports of differentially active proteins of a biochemical pathway could be achieved by regulations of the respective gene expressions.

We are thankful to Prof. L. S. B. Goldstein, UCSD, La Jolla, for his generosity and support. We also thank Prof.

P. Salvatera, Beckman Laboratories, USA, for a generous supply of fly stocks and antisera, and Prof. T Rosenberry, Miami, USA, and Prof. E. Buchner, University of Wuerzburg, Germany, for providing antibodies. This project was supported by an intramural fund from TIFR.

REFERENCES

Ahmari SE, Buchanan J, Smith SJ. 2000. Assembly of presynaptic active zones from cytoplasmic transport packets. Nat Neurosci 3:445–451.

Andres C, Beeri R, Friedman A, Lev-Lehman E, Henis S, Timberg R, Shani M, et al. 1997. Acetylcholinesterase-transgenic mice display embryonic modulations in spinal cord choline acetyltransferase and neurexin Ibeta gene expression followed by late-onset neuromotor deterioration. Proc Natl Acad Sci USA 94:8173–8178.

Berse B, Blusztajn JK. 1995. Coordinated up-regulation of choline acetyltransferase and vesicular acetylcholine transporter gene expression by the retinoic acid receptor alpha, cAMP, and leukemia inhibitory factor/ciliary neurotrophic factor signaling pathways in a murine septal cell line. J Biol Chem 270:22101–22104.

Bowman AB, Kamal A, Richtings BW, Philp A, McGrail M, Gindhardt JG, Goldstein LSB. 2000. Kinesin-dependent axonal transport is mediated by the sunday driver (SYD) protein. Cell 103:583–594.

Brown A. 2003. Axonal transport of membranous and nonmembranous cargoes: a unified perspective. J Cell Biol 160:817–821.

Carbini LA, Munoz Maines VJ, Salvaterra PM. 1990. Developmental expression of choline acetyltransferase mRNA in Drosophila. Neurochem Res 15:1089–1096.

Cervini R, Houhou L, Pradat PF, Bejanin S, Mallet J, Berrard S. 1995. Specific vesicular acetylcholine transporter promoters lie within the first intron of the rat choline acetyltransferase gene. J Biol Chem 270:24654–24657.

Di Giamberardino L, Couraud JY. 1978. Rapid accumulation of high molecular weight acetylcholinesterase in transected sciatic nerve. Nature 271:170–172.

Eaton BA, Fetter RD, Davis GW. 2002. Dynactin is necessary for synapse stabilization. Neuron 34:729–741.

Engel AG, Ohno K, Sine SM. 1999. Congenital myasthenic syndromes: recent advances. Arch Neurol 56:163–167.

Flybase: http://www.flybase.org.

Fonnum F, Frizell M, Sjostrand J. 1973. Transport, turnover and distribution of choline acetyltransferase and acetylcholinesterase in the vagus and hypoglossal nerves of the rabbit. J Neurochem 21:1109–1120.

Francis F, Roy S, Brady ST, Black MM. 2005. Transport of neurofilaments in growing axons requires microtubules but not actin filaments. J Neurosci Res 79:442–450.

He Y, Francis F, Myers KA, Yu W, Black MM, Baas PW. 2005. Role of cytoplasmic dynein in the axonal transport of microtubules and neurofilaments. J Cell Biol 168: 697–703.

ImageJ: http://www.rsb.info.nih.gov/ij/.

Incardona JP, Rosenberry TL. 1996. Replacement of the glycoinositol phospholipid anchor of Drosophila acetylcholinesterase with a transmembrane domain does not alter sorting in neurons and epithelia but results in behavioral defects. Mol Biol Cell 7:613–630.

Ito K, Hotta Y. 1992. Proliferation pattern of postembryonic neuroblasts in the brain of Drosophila melanogaster. Dev Biol 149:134–148.

Kasa P. 1968. Acetylcholinesterase transport in the central and peripheral nervous tissue: the role of tubules in the enzyme transport. Nature 218:1265–1267.

Kitamoto T, Wang W, Salvaterra PM. 1998. Structure and organization of the Drosophila cholinergic locus. J Biol Chem 273:2706–2713.

Kitamoto T, Xie X, Wu CF, Salvaterra PM. 2000. Isolation and characterization of mutants for the vesicular acetylcholine transporter gene in Drosophila melanogaster. J Neurobiol 42:161–171.

Koike H, Matsumoto H, Umitsu Y. 1989. Selective axonal transport in a single cholinergic axon of Aplysia—role of colchicine-resistant microtubules. Neuroscience 32:539–555.

Kondo S, Sato-Yoshitake R, Noda Y, Aizawa H, Nakata T, Matsuura Y, Hirokawa N. 1994. KIF3A is a new microtubule-based anterograde motor in the nerve axon. J Cell Biol 125:1095–1107.

Littleton JT, Chapman ER, Kreber R, Garment MB, Carlson SD, Ganetzky B. 1998. Temperature-sensitive paralytic mutations demonstrate that synaptic exocytosis requires SNARE complex assembly and disassembly. Neuron 21:401–413.

Lubinska L, Niemerco S, Oderfeld Nowak B, Szwarc L. 1964. Behavior of Acetylcholinesterase in Isolated Nerve Segments. J Neurochem 11:493–503.

Ohno K, Tsujino A, Brengman JM, Harper CM, Bajzer Z, Udd B, Beyring R, Robb S, Kirkham FJ, Engel AG. 2001. Choline acetyltransferase mutations cause myasthenic syndrome associated with episodic apnea in humans. Proc Natl Acad Sci USA 98:2017–2022.

Oosawa H, Fujii T, Kawashima K. 1999. Nerve growth factor increases the synthesis and release of acetylcholine and the expression of vesicular acetylcholine transporter in primary cultured rat embryonic septal cells. J Neurosci Res 57:381–387.

Parsons SM, Prior C, Marshal IG. 1993. Acetylcholine transport, storage and release. Int Rev Neurol 35:280–390.

Ray K, Perez SE, Yang Z, Xu J, Ritchings BW, Steller H, Goldstein LS. 1999. Kinesin-II is required for axonal transport of choline acetyltransferase in Drosophila. J Cell Biol 147:507–518.

Rosenbaum JL, Witman GB. Intraflagellar transport. 2002. Nat Rev Mol Cell Biol 3:813–825.

Roy S, Coffee P, Smith G, Liem RKH, Brady ST, Black MM. 2000. Neurofilaments are transported rapidly but intermittently in axons: implications for slow axonal transport. J Neurosci 20:6849–6861.

Sambrook J, Fritsch EF, Maniatis T. 1986. Molecular Cloning—A Laboratory Manual (2nd edition). Cold Spring Harbor Laboratory Press. (B.12).

Sarpal R, Ray K. 2002. Dynamic expression pattern of kinesin accessory protein in Drosophila. J Biosci 27: 479–487.

Sarpal R, Todi SV, Sivan-Loukianova E, Shirolikar S, Subramanian N, Raff EC, Erickson JW, Ray K, Eberl DF. 2003. Drosophila KAP interacts with the kinesin II motor subunit KLP64D to assemble chordotonal sensory cilia, but not sperm tails. Curr Biol 13:1687–1696.

Setou M, Seog DH, Tanaka Y, Kanai Y, Takei Y, Kawagishi M, Hirokawa N. 2002. Glutamate-receptor-interacting protein GRIP1 directly steers kinesin to dendrites. Nature 417:83–87.

Shiff G, Morel N. 1997 Rapid anterograde axonal transport of the syntaxin-SNAP 25-VAMP complex. J Neurochem 68:1663–1667.

Snow JJ, Ou G, Gunnarson AL, Walker MR, Zhou HM, Brust-Mascher I, Scholey JM. 2004. Two anterograde intraflagellar transport motors cooperate to build sensory cilia on C. elegans neurons. Nat Cell Biol 6:1109–1113.

Strausfeld N. 1976. Atlas of an insect brain. Berlin: Springer.

Suzuki M, Desmond TJ, Albin RL, Frey KA. 2001. Vesicular neurotransmitter transporters in Huntington's disease: initial observations and comparison with traditional synaptic markers. Synapse 41:329–336.

Takagawa K, Salvaterra PM. 1996. Analysis of choline acetyltransferase protein in temperature sensitive mutant flies using newly generated monoclonal antibody. Neurosci Res 24:237–243.

Torres JC, Behrens MI, Inestrosa NC. 1983. Neural 16S acetylcholinesterase is solubilized by heparin. Biochem J 215: 201–204.

Truman JW. 1990. Metamorphosis of the central nervous system of Drosophila. J Neurobiol 21:1072–1084.

Truman JW, Bate M. 1988. Spatial and temporal patterns of neurogenesis in the central nervous system of Drosophila melanogaster. Dev Biol 125:145–157.

Truman JW, Talbot WS, Fahrbach SE, Hogness DS. 1994. Ecdysone receptor expression in the CNS correlates with stage-specific responses to ecdysteroids during Drosophila and Manduca development. Development 120:219–234.

Tucek S. 1975. Transport of choline acetyltransferase and acetylcholinesterase in the central stump and isolated segments of a peripheral nerve. Brain Res 86:259–270.

Verhey KJ, Meyer D, Deehan R, Blenis J, Schnapp BJ, Rapoport TA, Margolis B. 2001. Cargo of kinesin identified as JIP scaffolding proteins and associated signaling molecules. J Cell Biol 152:959–970.

Wang L, Brown A. 2001. Rapid intermittent movement of axonal neurofilaments observed by fluorescence photobleaching. Mol Biol Cell 12:3257–3267.

Wang L, Brown A. 2002. Rapid movement of microtubules in axons. Curr Biol 12:1496–1501.

Wang L, Ho CL, Sun D, Liem RKH, Brown A. 2000. Rapid movement of axonal neurofilaments interrupted by prolonged pauses. Nat Cell Biol 2:137–141.

Wooten GF, Cheng CH. 1980. Transport and turnover of acetylcholinesterase and choline acetyltransferase in rat sciatic nerve and skeletal muscle. J Neurochem 34:359–366.

Xia CH, Roberts EA, Her LS, Liu X, Williams DS, Cleveland DW, Goldstein LS. 2003. Abnormal neurofilament transport caused by targeted disruption of neuronal kinesin heavy chain KIF5A. J Cell Biol 161:55–66.

Yamazaki H, Nakata T, Okada Y, Hirokawa N. 1995. KIF3A/B: a heterodimeric kinesin superfamily protein that works as a microtubule plus end-directed motor for membrane organelle transport. J Cell Biol 130:1387–1399.

Yang Z, Goldstein LS. 1998. Characterization of the KIF3C neural kinesin-like motor from mouse. Mol Biol Cell 9:249–261.

Yonekawa Y, Harada A, Okada Y, Funakoshi T, Kanai Y, Takei Y, Terada S, Noda T, Hirokawa N. 1998. Defect in synaptic vesicle precursor transport and neuronal cell death in KIF1A motor protein-deficient mice. J Cell Biol 141:431–441.

Zador E, Budai D. 1994. Expression of the acetylcholinesterase gene during development of Drosophila embryos. Neurobiology (Bp) 2:301–309.

Zinsmaier KE, Eberle KK, Buchner E, Walter N, Benzer S. 1994. Paralysis and early death in cysteine string protein mutants of Drosophila. Science 263:977–980.